Romanian Reports in Physics, Vol. 65, No. 1, P. 230–245, 2013

MODELING OF ATMOSPHERIC GLOW DISCHARGE CHARACTERISTICS

M. MANKOUR[1], A. W. BELARBI[2], K. HARTANI[3]

[1, 2] University of Sciences and Technology of Oran, Faculty of Electrical Engineering, Department of Electechnical, Algeria
E-mail: mohamed_mdz2000@yahoo.fr; Email: baw_dz@yahoo.com
[3] University of Saida, Faculty of Science and Technology, Department of Electechnical, Algeria
E-mail: kada_hartani@yahoo.fr

Received January 4, 2012

Abstract. The glow discharge in pure helium at atmospheric pressure is investigated and based on one-dimensional self-consistent fluid model. By solving the continuity equations for electrons, ions, and excited atoms, with the current conservation equation and the electric field profile, the time evolution of the discharge current, gas voltage and the surface density of charged particles on the dielectric barrier are calculated. The simulation results show that the peak values of the discharge current, gas voltage and electric field in the first half period are asymmetric to the second half. When the current reaches its positive or negative maximum, the electric field profile, and the electron and ion densities represent similar properties to the typical glow discharge at low pressures

Key words: atmospheric pressure glow discharge, numerical simulation, helium gas.

1. INTRODUCTION

The present work deals with a numerical study of glow discharge set up in the helium atmospheric pressure. This study consists of developing a mono-dimensional numerical model with the aim to examine the properties of this discharge.

The applicant's field of this process is a very wide [1]. Ozone generation processing of gaseous effluents, activation and processing of surface, CO2 laser, lamp excimer, plasma screens etc. and has to do with a numerous industrial domains: electronics, textile, packaging car and manufacturing.

In recent years many studies have been concerned with the effects of gas flow and electrode geometry on the discharge mode and characteristics. While several authors have published experimental and modeling studies of plane-parallel DBD at atmospheric pressure, under specific conditions, for instance, at least one of

electrodes covered with a dielectric layer, an ac power with an appropriate frequency, etc., atmospheric pressure glow discharges (APGD) is obtained relatively readily in helium. Helium APGD has been studied extensively. For simplicity, many theoretical studies made an approximation that the average electron energy is constant throughout the discharge space at any time; the value of electron energy is chosen empirically.

The line of works in the glow discharge with dielectric barrier is to turn towards a very detailed modeling of the discharge, a good modeling makes it possible to understand and predict their behavior, [2–9] then the control and use of this technology in industrial needs, such as semi-conductors, panels of plasma visualization, the deposit of the thin layers, the die-sinking in micro-electronics and the treatment of surfaces [10–14].

2. PHYSICAL MODEL

The functioning of this discharge which is similar to all these discharge, in gas, is governed and directed by a multitude of different physical phenomenon from one to another but strongly coupled.

It is thus necessary to consider the system on the whole, and then to work out (carry out) a self-coherent modeling able to take into account the coupling between the conveyance of charged particles and the kinetics of the existing states on the one hand and the electrical field on the other hand.

The model thus being developed allows understanding well the functioning of the discharge.

Under study attempting to reproduce from the description of the involved basic physical phenomena (phenomena of electronic and ionic conveyance in gas, electrical field) is an electrical characteristics of the discharge. These characteristics do not inform us about the intervening whole of the phenomena during the discharge.

The use of the helium, within the framework of this study, is one of the conditions of the obtainment of a glow rate of charge atmospheric pressure of gas, mainly characterized by its metastable levels of potential high-energy and by its weak potential of rupture.

The reaction taken into account in the numerical modeling and putting in plays the electrons, the ions and the natural excited particles are represented as shown in Fig. 1 [15].

Have reaction rates (of which certain are presented in Figure 1) is constant depending on the electric field. The knowledge of these factors which control the density of different particles is necessary to understand and to describe the discharge.

3. MATHEMATICAL MODEL

The finest theoretical description of the particles behavior which characterizes the functioning of an electrical discharge requires the resolution of the kinetics equations as a whole (frequency called equation of discharge particle conveyance) associated at each one of these particles.

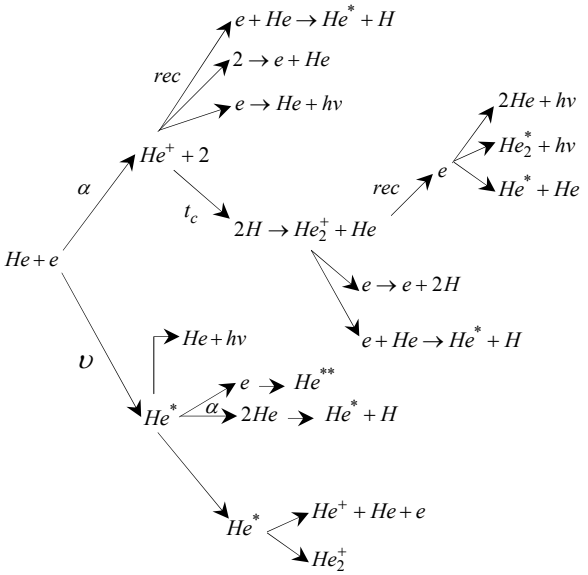

Fig. 1 – The process of reaction and the disappearance of different particles.

Fundamental equation rendering account of the space and temporal evolution of particles density is the equation of continuity that globally takes the same form for electrons and ions. We get the following equations:

- for the electrons

$$\frac{\partial ne(\vec{r},t)}{\partial t} + \frac{\partial(\vec{w}_e(\vec{r},t)n_e(\vec{r},t))}{\partial \vec{r}} - \frac{\partial}{\partial \vec{r}}\left[\vec{D}_e(\vec{r},t)\frac{\partial n_e(\vec{r},t)}{\partial \vec{r}}\right] = s_e(\vec{r},t); \tag{1}$$

- for the ions

$$\frac{\partial ni(\vec{r},t)}{\partial t} + \frac{\partial(\vec{w}_i(\vec{r},t)n_i(\vec{r},t))}{\partial \vec{r}} - \frac{\partial}{\partial \vec{r}}\left[\vec{D}_i(\vec{r},t)\frac{\partial n_i(\vec{r},t)}{\partial \vec{r}}\right] = s_i(\vec{r},t); \tag{2}$$

- for the excited particles

$$\frac{\partial n_m(\vec{r},t)}{\partial t} - \frac{\partial}{\partial \vec{r}}\left[\vec{D}_m(\vec{r},t)\frac{\partial n_m(\vec{r},t)}{\partial \vec{r}}\right] = S_m(\vec{r},t), \tag{3}$$

which permit to determine the space temporal evolution of the electronic and ionic densities subject to the knowledge of the running back speed, diffusion coefficient and frequencies of ionization of each charged particle.

The three aforementioned equations above are named convection-diffusion equation for they are composed of the term convective (of the 1st rank with regard to the space shunted) and the term of diffusion (of the 2nd rank with regard to the space shunted).

In glow discharge, the space charge due to the ions and electrons presence is sufficient to distort the geometrical electric field. This phenomenon should be described by coupling the equations of electric and ionic conveyance with the equation of Poisson for the electric field, the equation of Poisson is written as:

$$\vec{\nabla}\varepsilon_r E = \frac{e}{\varepsilon_0}(n_i - n_e - n_n). \tag{4}$$

The equation of Boltzmann is coupled with to the one of Poisson from an auto coherent electrical model of the discharge.

3.1. MACROSCOPIC APPROACH (FLUID MODELS)

The conveyance of the charge particles is in this approach characterized by average size then the density, the average speed and average energy of the particles.

The equation of Boltzmann is then substituted by three equations which describe the space-temporal evolution of three average values.

3.2. FLUID MODEL WITH THE TWO MOMENTS

The developed model in this research is based on the resolution of first two moments of Boltzmann's equation in this model, the first 2 conveyance equations are:

- Continuity equation;
- Conveyance equations of the quantity of movement are coupled to the Poisson equation. To be able to suppress the equation of energy, it is necessary to use the local field approximation.

The numerical model developed in this research is fluid and mono-dimensional. The aim of a fluid model is to give the appropriate qualitative tendencies which enable us to know the preponderant physical phenomena that affect the discharge at the level of the actuator DBD.

3.3. SOURCE TERMS OF CONVEYANCE EQUATIONS

The expressions of the source terms of electrons, ions and of the metastable contain the reactions rates (noted k_i) and the ionization frequencies and excitation besides the different particle density [13], [17].

▪ **Electron**

$$\begin{aligned} S_e = \nu n_e + n_{x1}\left(k_{11} n_{x1}\right) - n_{p1} n_e \left(k_4 + k_5 n_e + k_6 n_{He}\right) \\ - N_{p2} n_e \left(k_7 + k_8 + k_2 n_{He} + k_9 n_e\right) - n_{p3} n_e \left(k_{10} + k_{11} n_e\right); \end{aligned} \tag{5}$$

▪ **Atomic ions** He^+

$$S_{p1} = \nu n_e + k_{11}\left(n_{x1}\right)^2 - n_{p1} n_e \left(\left(k_4 + k_5 n_e + k_6 n_{He}\right) - n_{p1} k_1 \left(n_{He}\right)^2\right); \tag{6}$$

▪ **Molecular ions** He_2^+

$$S_{p2} = n_{p1} k_1 \left(n_{He}\right)^2 - n_{p2} n_e \left(k_2 n_{He} + k_7 + k_8 + k_9 n_e\right); \tag{7}$$

▪ **Source term of the excited species** $He\left(2^3S\right)$

$$S_{x1} = \nu_1 n_e + n_{p2} n_e k_8 - n_{x1}\left(k_3 \left(n_{He}\right)^2 + k_{10} n_e + k_{11} n_{x1}\right), \tag{8}$$

where n_e, n_{p1}, n_{p2}, n_{He} designate respectively the density of the electrons atomic and molecular ions of helium, where n_{x1} designates (indicates) the helium density, and $He\left(2^3S\right)$ the charged particles, the rates k_i are defined in Table 1 [7, 18–20].

Table 1

Assessment of the reactions in Helium

Reaction	Symbol	Rate of reaction
Reaction to three bodies		
$He^+ + 2He \rightarrow He_2^+ + He$	k_1	$6.3 \times 10^{-32} cm^6 s^{-1}$
$He_2^+ + e + He \rightarrow He_2^* + He$	k_2	$5 \times 10^{-27} cm^6 s^{-1}$
$He\left(2^3S\right) + He \rightarrow He_2^* + He$	k_3	$2.5 \times 10^{-34} cm^6 s^{-1}$
Recombination		
$He^+ + e \rightarrow He + \boldsymbol{h\nu}$	k_4	$2 \times 10^{-12} cm^6 s^{-1}$
$He^+ + 2e \rightarrow He + e$	k_5	$7.1 \times 10^{-20} cm^6 s^{-1}$
$He^+ + e + He \rightarrow He^* + He$	k_6	$1 \times 10^{-27} cm^6 s^{-1}$
$He_2^+ + e \rightarrow He_2^* + \boldsymbol{h\nu}$	k_7	$5 \times 10^{-10} cm^6 s^{-1}$

Table 1 (continued)

$He_2^+ + e \rightarrow He(2^3S) + He$	k_8	5×10^{-9} cm^{6}s^{-1}
$He_2^+ + e \rightarrow 2He + e$	k_9	2×10^{-20} cm^{6}s^{-1}
Reaction to two bodies		
$He(2^3S) + e \rightarrow He + e$	k_{10}	2.9×10^{-9} cm^{6}s^{-1}
$He(2^3S) + He(2^3S) \rightarrow e + He^+ + He$	k_{11}	2.9×10^{-9} cm^{6}s^{-1}

4. NUMERICAL MODEL

We solve the continuity equation from the method of the finished differences based on the discretization diagram of Sharfetter and Gummel [21]. Its main advantage is related to its stability and to the fact that it can deliver, in a continuous manner a situation in which either the term "Shunt", or the term diffusion of the current of the charged particle is dominant. This diagram enables us to discredit implicitly the equation of continuity and to break loose from constraints of pace in time imposed in the case of explicit discretization.

The discretization of density of the charged particles and the flux as well as that of the Poisson equation is as follows.

4.1. DISCRETIZATION OF THE CONVERGENCE EQUATIONS

Generally, we can not solve the heavily coupled systems, constituted of the first two instants of Boltzmann's equation and of Poisson's one in a simple and direct manner. The problem is then to draw as near as necessary the exact values to the solution. The chosen method is the method of the finished differences according to the diagram of Sharfetter and Gummel [21] for the developed conveyance at the lead for semi-conductors modeling.

4.2. DISCRETIZATION OF THE DENSITY OF THE CHARGED PARTICLES AND OF THE FLUX

The densities of the charged particles are defined at the (i, j) cell core, Figure 2. In the equation of continuity and in the transfer of the movement quantity, the flux of the charged particles following the X axe and the one of the Y are defined between the (i, j) and $(i+1, j)$ and (i, j) and $(i, j+1)$ points respectively and then, notice:

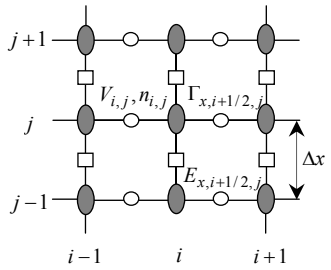

Fig. 2 – Used maillage in the model.

In this method of Sharfetter and Gummel, we suppose that the particle flux is constant between two successive nodes of the maillage. This diagram is advantageous for the integration of the conveyance equation is analytic, which confers (bestows) it a very good stability.

For instance, we start from following conveyance equation *X*:

$$\Gamma = s\frac{\mu E}{D}(nD) - \frac{\partial(nD)}{\partial x}. \tag{9}$$

μ and D are the mobility and the diffusion coefficient, *S* is equal to –1 and 1 respectively for the electrons and the ions. We find as solution:

$$nD = s\frac{D}{\mu E}\Gamma + C\exp\left(s\frac{\mu E}{D}x\right). \tag{10}$$

The densities of the charged particles are defined at the center of (i, j) cells. We will have, for example, the same value $\Gamma x, i+1/2, j$ of the flux between (i, j) and $(i+1, j)$ nodes. As soon as, the discretization *n* following the finished difference gives off:

$$n_{i,j}D_{i,j} = s\frac{D_{i+1/2,j}}{\mu_{i+1/2,j}.E}\Gamma_{i+1/2,j} + C\exp\left(s\frac{\mu_{i+1/2,j}.E_{i+1/2,j}}{D_{i+1/2,j}}x_{i,j}\right), \tag{11}$$

$$n_{i+1,j}D_{i+1,j} = s\frac{D_{i+1/2,j}}{\mu_{i+1/2,j}.E}\Gamma_{i+1/2,j} + C\exp\left(s\frac{\mu_{i+1/2,j}.E_{i+1/2,j}}{D_{i+1/2,j}}x_{i,j}\right). \tag{12}$$

If we subtract (11), (12), we obtain C

$$C\exp\left(s\frac{\mu_{i+1/2,j}.E_{i+1/2,j}}{D_{i+1/2,j}}x_{i,j}\right) = \frac{n_{i+1,j}D_{i+1,j} - n_{i,j}D_{i,j}}{\exp\left(s\frac{\mu_{i+1/2,j}.E_{i+1/2,j}}{D_{i+1/2,j}}\right) - 1}, \tag{13}$$

paying

$$Z_{i+1/2,j} = s\frac{\mu_{i+1/2,j}E_{i+1/2,j}}{D_{i+1/2,j}}\Delta x_{i,j}. \tag{14}$$

The expression of the following flux X is written in the discretization of the finished differences, according to the exponential diagram of Sharfetter and Gummel as follows:

$$\Gamma_{x,i+1/2,j} = -\frac{1}{x}D_{i+1/2}\left(f_1\left(z_{x,i+1/2,j}\right)n_{i+1,j} - f_2\left(z_{x,i+1/2,j}\right)n_{i,j}\right). \tag{15}$$

After $f_1(2)$ and $f_2(2)$ defined by

$$f_1(z) = \frac{z}{\exp(z)-1}, \tag{16}$$

$$f_2(z) = \frac{z\exp(z)}{\exp(z)-1} = f_1(z) + z. \tag{17}$$

For $z \neq 0$, and $f_1(0) = f_2(0) = 1$ the expression of flux (the flux expression) in the Y direction has the same form.

We replace in the equation of continuity the flux by their expression which is a linear combination of densities and we obtain the following equation which is a linear combination between the five neighbors' points.

$$a_{i,j}^E n_{i+1,j} + a_{i,j}^w n_{i-1,j} + a_{i,j}^N n_{i,j+1} a_{i,j}^s n_{i,j-1} + a_{i,j}^c n_{i,j} = A_{i,j}. \tag{18}$$

The coefficients inside the simulation field are defined by:

$$a_{i,j}^E = -\frac{2.\Delta t.D_{i+1/2,j}}{\Delta x_i(\Delta x_i + \Delta x_{i-1})} f_1(z_{x,i+1/2,j}), \tag{19}$$

$$a_{i,j}^w = -\frac{2.\Delta t.D_{i-1/2,j}}{\Delta x_{i-1}(\Delta x_i + \Delta x_{i-1})} f_2(z_{x,i-1/2,j}), \tag{20}$$

$$a_{i,j}^N = -\frac{2.\Delta t.D_{i,j+1/2}}{\Delta y_{j+1}(\Delta y_j + \Delta y_{j-1})} f_1(z_{y,i,j+1/2}), \tag{21}$$

$$a_{i,j}^s = -\frac{2.\Delta t.D_{i,j-1/2}}{\Delta y_{j-1}(\Delta y_i + \Delta y_{i-1})} f_1(z_{y,i,j-1/2}), \tag{22}$$

$$a_{i,j}^c = 1 - a_{i-1,j}^E - a_{i+1,j}^w - a_{i,j-1}^N - a_{i,j+1}^s, \tag{23}$$

$$A_{i,j} = n_{i,j}^k + \Delta t S_{i,j}. \tag{24}$$

For the surface (space) between dielectric and gas, the expression of the electronic flux is defined by:

$$(\Gamma_e n)_{i,j} = a_{i,j}\mu_{i,j}E_{i,j}n_{i,j} + \frac{v_{th,i,j}n_{i,j}}{4} - \gamma(\Gamma_p n)_{i,j}, \tag{25}$$

And the coefficient expressions are:

$$a^E_{i,nd} = a^w_{i,nd} = a^s_{i,nd} = 0, \tag{26}$$

$$a^n_{i,nd} = -\frac{2\Delta t D_{i,j+1/2}}{\Delta y_{nd}} f_1(z_{y,i,j+1/2}), \tag{27}$$

$$a^c_{i,j} = 1 - a^N_{i,j-1} + \frac{2\Delta t}{\Delta y_{nd}} a_{i,nd}.\mu_{i,j}.E_{y,i,nd} + \frac{2\Delta t}{\Delta y_{nd}}\nu_{th}, \tag{28}$$

$$a^c_{i,j} = 1 - a^E_{i-1,j} - a^w_{i+1,j} - a^N_{i,j-1} - a^s_{i,j+1}. \tag{29}$$

Discretization of the Poisson's equation

$$\vec{\nabla}\varepsilon_r E = \frac{e}{\varepsilon_0}(n_i - n_e). \tag{30}$$

In the discretization of the finished differences, the "Laplacian" of the potential is written:

$$\frac{\partial^2 V}{\partial x^2}\Big|_{i,j} = \frac{V_{i+1,j} + V_{i-1,j} - 2V_{i,j}}{\Delta x^2}, \tag{31}$$

$$\frac{\partial^2 V}{\partial y^2}\Big|_{i,j} = \frac{V_{i,j+1} + V_{i,j-1} - 2V_{i,j}}{\Delta y^2}. \tag{32}$$

– *Conditions to the limits*. We assume that the flux of the charged particles towards the sides of the field of simulation is worthless (nul) that we translate it by the conditions to the symmetric limits $\Gamma_e \vec{n} = 0$. But the flux of the charged particles towards the dielectric is written under the form:

$$\varphi_{e,i} = An_{e,i}w_{e,i} + \frac{n_{e,i}v_{th,e,i}}{4}, \tag{33}$$

with $\boldsymbol{w_{e,i}} = \pm\mu_{\boldsymbol{e,i}}\boldsymbol{E}$. $n_{e,i}$ is the electrons or ions (i) density at the surface of the side, $w_{e,i}$ the derive speed is a parameter equal to 1 if $w_{e,i}$ is directed towards the side if not equal to zero.

Table 2

Transport parameters used in Helium

Transport parameter	Values
Ions mobility μ_i	$= (8\times10^3/p)1\text{-}8\times10^{-3}\ E/p$ cm^{2}V^{-1}s^{-1} For $E/p \le 25$cm^{-1}torr^{-1} $=(4{,}1\times10^4/p\sqrt{E/p}\ [1\text{-}27.44/E/p^{1.5}]$cm^{2}V^{-1}s^{-1} For $E/p > 25$cm^{-1}torr^{-1}
Electrons mobility μ_{ie}	$=(e/m_e\upsilon_{en})$cm^{2}V^{-1}s^{-1} and $\upsilon_{en}=10^2$ /s
Ions diffusion D_i	$=500$cm^2/s
Electrons diffusion D_e	$=(KT_e/e)\ \mu_e$ cm^2/s

5. RESULTS AND DISCUSIONS

In our model, the series of equations above are solved numerically, and discretization of Eq. (1), (2), (3) and (4) is performed in accordance with semi-implicit Scharfetter-Gummel scheme [21]. The mobility and diffusion coefficient used are the same as those in [22–23]. The photo–ionization contribution is not taken into account in this model. As the initial condition, we assume that the electron density and the atomic ion density are equal to each other and uniformly distributed in the discharge region $n_e(r,0) = n_i(r,0) = 10^7$ cm^{-3}, while the molecular ion density and the excited atom density are both 10^2 cm^{-3}. The spacing between the two electrodes is 6 mm; a sinusoidal voltage is externally applied to the inner electrode, its amplitude and frequency are 2 KV and 50 KHz respectively.

Figures 3, 4 and 5 show the temporal evolution of the total discharge current, the gas voltage during a typical cycle and current density. It can be seen that there is one current peak in each half cycle of the applied voltage. Different from the parallel-plate configuration, the current peak in various half periods loses its original shape. The current maximum of 0.0022A in the first half is different from the second, which is only –0.0062A. In addition, the pulse width of the discharge current in the latter half period is wider than that in the former. It is due to the fact that in the first half, the discharge cathode is the outer electrode with a big radius so that the volume of ionization region in the cathode sheath is also very large, leading to a strong current gathering; while in the latter half period, the discharge cathode is the inner wire electrode with a very much smaller radius. Although in the latter case the sheath electric field is much stronger than that in the former, the volume of the ionization region is however so small that it leads to a smaller current peak. The blue line in Fig. 3 represents the time evolution of the gas voltage with the applied voltage during a typical cycle. At the initial moment, the applied voltage is zero, and the gas voltage is not zero but equal to the memory voltage produced by the charged particles accumulated on the dielectric. As the applied voltage rises, the gas voltage increases until it reaches the breakdown voltage. Then the gas is punctured and discharge starts. Meanwhile, the charges accumulated on the dielectric produce a reverse electric field, making the gas voltage drop and

leading to a termination of the gas discharge. In the latter half period, due to the reversal of the applied voltage, the electric field produced by the accumulated charges has the same direction as the applied field, so it reduces the threshold applied voltage for starting the next discharge. Furthermore, since the breakdown during the latter half period happens in the cathode sheath near the inner wire electrode, where the electric field is strong, correspondingly it is easier to puncture, and therefore the breakdown voltage in the latter half period is lower than that in the former half period. As a result of the higher discharge current during the former half period, the accumulation seed of charged particles on the dielectric barrier is fast too. Then the gas voltage drops rapidly and the discharge is suppressed quickly, and consequently the discharge current pulse is narrow. However, during the latter half period, since the discharge current is low, the accumulation speed of charged particles on the dielectric is also low. Thus the gas voltage changes slowly and its suppressing effect on discharge is small, so the current pulse is wide.

Figures 6, 7, 8, 9, 10 and 11 illustrate the spatial distributions of the electric field, the electron, and the ion as well as the excited atom densities when the discharge current reaches its positive or negative maximum during the cycle. When the discharge happens in the former half period, the cathode sheath is formed near the dielectric barrier covering the outer electrode. There obviously exist a cathode fall, a negative glow region, a Faraday dark region, and a plasma positive column. This shows a similar feature to the typical glow discharge at low pressures. In the cathode fall, the electric field can be up to 260V/cm and then decreases linearly from the cathode. The maximal ion density in this region is $4.5 \cdot 10^8$ cm^{-3} and the width of the cathode fall is about 0.5 mm. The width of the negative glow region and the faraday dark region is about 2.5 mm. The electron density shows a negative glow region with a peak value of $4.3 \cdot 10^8$ cm^{-3}. In other words, when the current reaches a peak during the former half period, the maximal electron density does not occur near the sheath but near the inner electrode. Due to the axial symmetry, the current density near the inner wire electrode is the highest. In the plasma positive column, the electric field is quite low, about 30V/cm. The electron and ion densities are nearly equal to each other. Due to the asymmetry of discharges, the densities are not uniform in the plasma region but increase gradually from the outer to the inner electrode. Latter half period when the current reaches the maximum, the cathode sheath is formed near the inner electrode. Obviously there exist the cathode fall, the negative glow region, and the positive column. In the cathode sheath, the electric field intensity is 285V/cm in maximum and shows a tendency to reduce linearly. The thickness of the sheath is about 0.3 mm and the ion density can be up to $4.7 \cdot 10^8$ cm^{-3}. The maximal electron density of $4.9 \cdot 10^8$ cm^{-3} appears at the boundary near the sheath. In the plasma positive column, the electric field intensity is small and keeps almost steady; while the electron and ion density are equal to each other, $4.5 \cdot 10^8$ cm^{-3}. The distribution of the excited atom density does not change too much during the former and the latter half period. The maximal densities (about $1 \cdot 10^7$ cm^{-3}) both appear in the region near the inner wire electrode. The excited atom density decreases in the direction from the inner to the outer electrode.

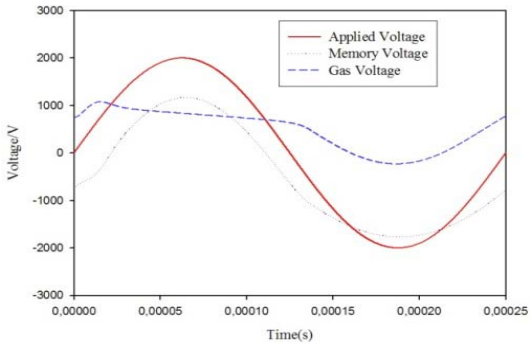

Fig. 3 – Evolution of the gas voltage in typical cycle.

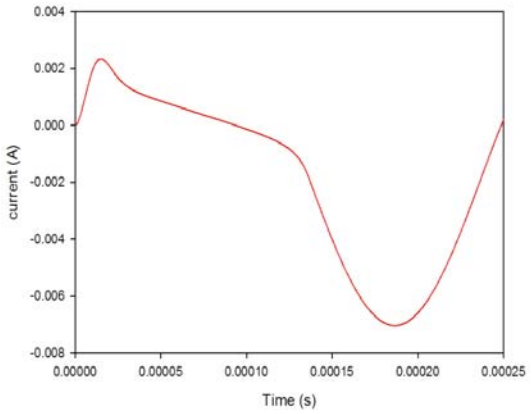

Fig. 4 – Evolution of the total discharge current in typical cycle.

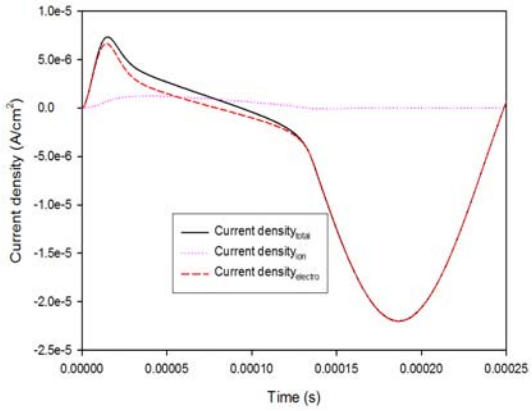

Fig. 5 – Evolution of the current density in typical cycle.

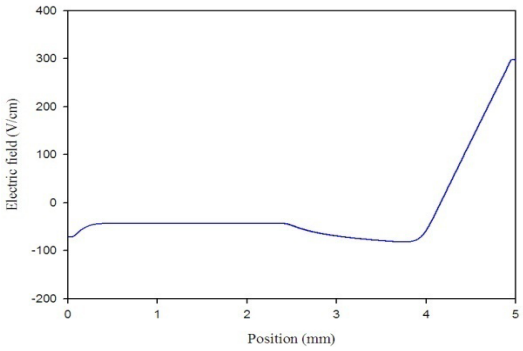

Fig. 6 – The spatial distribution of the electrical field.

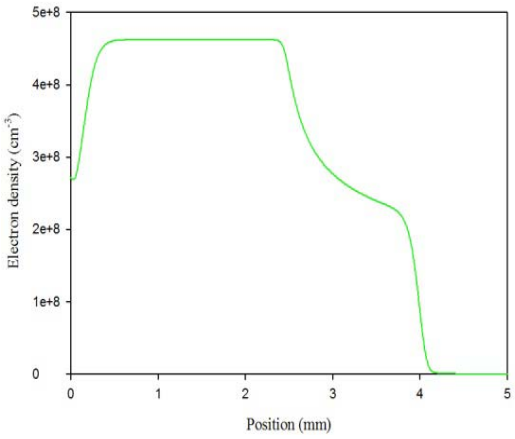

Fig. 7 – The spatial distribution of electron density.

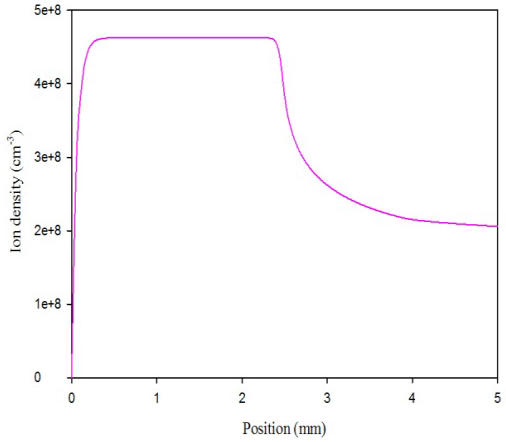

Fig. 8 – The spatial distribution of ion density.

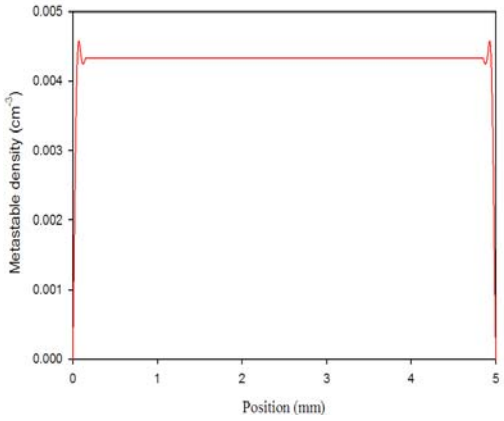

Fig. 9 – The spatial distribution of metastable density.

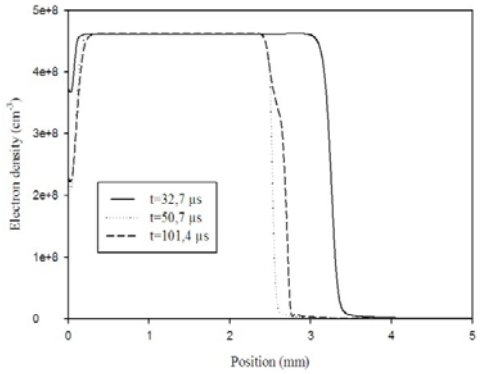

Fig. 10 – The spatial distribution of electron density in t = 32.7μs, t = 50.7μs and t = 101.4μs.

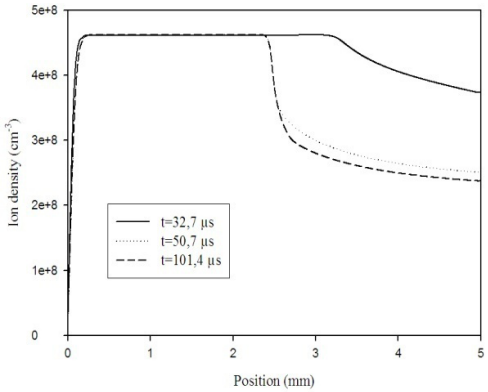

Fig. 11 – The spatial distribution of ion density in t = 32.7μs, t = 50.7μs and t = 101.4μs.

6. CONCLUSION

Based on the one-dimensional and self-consistent fluid model, the characteristics of the dielectric barrier glow discharge in pure helium at atmospheric pressure generated between two coaxial electrodes is investigated numerically. In calculation, we have considered the elementary ionization and excitation processes in pure helium. Under the drift-diffusion approximation, by solving the one-dimensional continuity equations for electrons, ions and excited atoms, together with the current conservation equation, the simulation results show the spatial-temporal distributions of the electric field and the electron, ion and excited atom densities, as well as the time evolutions of the discharge current and the gas voltage. At maximal discharge current, there obviously exist the cathode fall, the negative glow region and the positive column, similar to the APGD with the dielectric barrier between parallel-plate electrodes. The simulation results reveal that the peak discharge current, gas voltage and the electric field are asymmetric by comparing the first half cycle with the second. The influence of the way the dielectric covers the electrodes on discharge current characteristics is very significant.

REFERENCES

1. Kogelshtz U., *Dielectric-barrier discharges their history discharge physics and industrial applications*, Plasma chem. Plasma process, **33**, *1*, 1–46 (2003).
2. Roth JR, Sherman DM, and Wilkinson SP., *Boundary layer flow control with a one atmosphere uniform glow discharge*, 36th AIAA Aerospace Sciences Meeting and Exhibit, Reno, NV, AIAA paper 98-0328, Jan.12–15 (1998).
3. Corke TC, Jumper EJ, Post ML, Orlov D and Mclaughlin T., *Application of weakly-ionized plasmas as wing flow-control devices*, 41st Aerospace Sciences Meeting and Exhibit, AIAA paper 2002–0350, Reno, NV, Jan. 6–9 (2003).
4. Kim Y, Kang WS, Park JM, Hong SH, Song YH, and Kim SJ., *Experimental and numerical analysis of streamers in pulsed corona and dielectric barrier discharges*, IEEE Trans. Plasma Sci, **32**, *1*, 18–24 (2004).
5. Roth JR, Rahel J, Dai X, and Sheman DM., *The physics and phenomenology of one atmosphere uniform glow discharge plasma (OAUGDP) reactors for surface treatment applications*, J. Phys. D, Appl.Phys, **38**, *4*, 555–567 (2005).
6. Shenton MJ and Stevens GC., *Surface modification of polymer surfaces: Atmospheric plasma versus vacuum plasma treatments*, J. Phys. D, App. Phys., **34**, *18*, 2761–2768 (2001).
7. Golubovskii YB, Maiorov VA, Behnke J and Behnke JF., *Modeling of the homogeneous barrier discharge in helium at atmospheric pressure*, J. Phys. D, App. Phys., **36**, 39–49 (2003).
8. Tendero C, Tixier C, Tristant P, Desmaison J, Leprince P., *Atmospheric pressure plasmas,* Spectrochim. Acta, Part B, **61**, *7*, 2–30 (2006).
9. Massines F, Ségur P, Gherardi N, Khamphan C and Ricard A., *Physics and chemistry in a glow dielectric barrier discharge at atmospheric pressure: Diagnostics and modeling*, Surf. Coatings Technol., **8**, *14*,174–175 (2003).
10. Webb MR, Andrade FJ, Hieftje GM., *The annular glow discharge A small-scale plasma for solution analysis*, Anal. At. Spectrom, **22**, *7*, 775–782 (2007).

11. Montie TC, Kelly-Wintenberg K and Roth JR., *An overview of research using the one atmosphere uniform glow discharge plasma (OAUGDP) for sterilization of surfaces and materials*, IEEE Trans.Plasma Sci., **28**, *1*, 41–50 (2000).
12. Yang X., *Comparison of an atmospheric pressure, radio-frequency discharge operating in the α and γ modes*, Plasma Sources Sci., **19**, *2*, 314–320 (2005).
13. Massines F, Messaoudi R and Mayoux C., *Comparison between air filamentary and helium glow dielectric barrier discharges for the polypropylene surface treatment*, Plasmas Polym., **3**, *1*, 43–59 (1998).
14. Singh KP, Roy S and Gaitond DV., *Modeling of dielectric barrier discharge plasma actuator with atmospheric air chemistry*, 37th AIAA Plasma dynamics and lasers conference, AIAA paper 2006-3381, San Francisco, CA, Jun. 5–8 (2006).
15. Gadri RB., *One atmospheric glow discharge structure reveled by computer modeling*, IEEE Trans. Plasma Sci., **27**, *1*, 36–37 (1999).
16. Massines F, Rebehi A, Decomps P, Gadri RB, Ségur P and Mayoux C., *Experimental and theoretical study of a glow discharge at atmospheric pressure controlled by dielectric barrier*, J. App. Phys., **83**, *6*, 2950–2957 (1998).
17. Andrade FJ, Shelley JT, Wetzel WC, Webb MR, Gamez, G Hieftje SJ. *Atmospheric pressure chemical ionization source*, Anal.Chem, **80**, *8*, 2646–2653 (2008).
18. Hill PC and Heman PR, *Reaction processes in He^{+}_{2} flash lamp*, Phys. Rev, **47**, *6*, 4837–4844 (1993).
19. Quinteros T, Dewitt DR, Schuch R and Belkic D., *Recombination of D^{+} and He^{+} ions with low-energy free electrons*, Phys. Rev, **51**, 1340–1349 (1995).
20. Yuan X and Raja LL., *Computational study of capacitively coupled high-pressure glow discharges in helium*, IEEE Trans. Plasma Sci, **31**, *4*, 495–503 (2003).
21. Scharfettre DL and Gummel HK., *Large signal analysis of silicon read diode oscillator*, IEEE Trans. Electron devices ED-16, **64** (1969).
22. Roy S and Gaitonde DV., *Modeling surface discharge effects of atmospheric RF on gas flow control*, Proceeding 43rd AIAA aerospace Sciences meeting, **160**, 10–13 (2005).
23. Shi JJ and Kong MG., *Cathode fall characteristics in a dc atmospheric pressure glow discharge*, J. App. Phys., **94**, *9*, 5504–5513 (2003).